Title: "Joule heating in pores during electroporation is insufficient to disrupt the cell membrane"

Authors: Ting Shu[1], Quim Castellví[1], Antoni Ivorra[1,2]

[1]Department of Engineering, Universitat Pompeu Fabra, Barcelona

[2]Serra Húnter Programme, Universitat Pompeu Fabra, Barcelona

Corresponding Author: Antoni Ivorra

Keywords/search terms: electroporation, electropermeabilization, joule heating, mechanism study, numerical study.

Abstract

The electroporation phenomenon is not yet fully understood. In particular, it remains unclear why cell membrane permeability, as indicated by impedance measurements, continues to increase during electric field exposure and why elevated permeability persists long after the field has been removed. This study conducts a numerical investigation to determine whether Joule heating, which is expected to be intense within the pores formed during electroporation, can produce temperature increases sufficient to locally affect the structural integrity of the cell membrane, potentially serving as a contributing mechanism. To achieve this, an electroporated cell membrane patch containing one or more pores was modelled using the finite element method. The study first simulated the dynamic temperature increase resulting from the application of a 100 μs square electric pulse. Subsequently, static temperature distributions, corresponding to permanent field exposures, were analysed as a function of pore size, geometry, and density to explore their influence on temperature elevation. The results indicate that the temperature increases are minimal (< 0.1 K) and negligible with respect to membrane disruption, suggesting that Joule heating within pores is very unlikely to contribute to the electroporation phenomenon.

1. Introduction

Electroporation, also termed electropermeabilization, is a biophysical phenomenon in which the application of electric fields transiently increases the permeability of the cell membrane. Based on previous experimental measurements and theoretical and numerical studies [1–4], the most widely accepted mechanism underlying the electric field induced increases in membrane permeability is the transient formation of nanometer-sized aqueous pores in the lipid bilayer due to the elevated transmembrane voltage during electric field exposure.

It is believed that pores are generated at the onset of electric pulse with most closing immediately upon pulse cessation with transient closure time, while a small portion of these pores remain open for hundreds of seconds after pulse [5–8]. However, current models for pore formation, growth, and annihilation exhibit limitations when researchers attempt to explain the slow increase in permeability during electroporation and the post-pulse molecular uptake [9,10]. Specifically, during exposure to a sequence of electric pulses, the cell membrane exhibits a gradual rise in permeability during and with each subsequent pulse, following a rapid increase at the onset of the first pulse [11–14]. Additionally, molecular transport experiments indicate that molecular uptake does not immediately cease after the electric field ends, but continues at a slower rate. Over time, the permeability gradually returns to its original value, and molecular uptake eventually ceases [9,10,15,16].

Efforts have been made to explore explanations other than pore formation for the permeability increase induced by electric fields. One of the possible mechanisms discussed in previous studies is lipids peroxidation. Results from a molecular dynamic simulation study by Rems et. al. in 2018 indicate that hydroperoxide lipid derivatives can only account for the lowest values of permeability and conductivity measured experimentally. This suggests that oxidized membrane lesions may contribute to ionic transport after the closure of pores but they cannot be the only mechanism [17].

Taking into account these observations, and particularly the continued increase in membrane permeability during electric field exposure as indicated by impedance measurements[11], we considered the possibility that Joule heating, which is expected to be especially intense within the pores formed during electroporation, may produce localized temperature elevations

sufficient to compromise the structural integrity of the cell membrane, thereby potentially contributing to the electroporation pehnomenon. This conjecture would be supported by observations obtained, at a larger scale, in the context of skin electroporation. Researchers of skin electroporation found µm-sized regions of increased permeability with low-voltage long-duration pulses applied and attributed the permeability increase to the lipid phase transition due to Joule heating induced local temperature elevating (i.e., over 65 °C) in Stratum Corneum (SC) [18–20].

To assess the validity of our conjecture, we have conducted a numerical study. In this numerical study, we built a 3D model to simulate the Joule heating and thermal conduction in a patch of electroporated cell membrane. We firstly analyzed the dynamic temperature increase throughout the entire electric field. Subsequently, since cylindrical pores formed under an electric field initially exhibit an arc-shaped profile with a narrow central pathway-and because these pores typically develop asymmetrically at the anode and cathode poles [10,21–24] -we conducted static simulations to examine the temperature increase under different pore sizes, geometries, and densities.

2. Materials and methods

2.1 Elecctroporated cell membrane patch

To investigate the thermal effects on electropermeabilization resulting from electroporation, we considered a scenario in which an aqueous pore forms on a cell membrane patch due to exposure to an electric field, with the field remaining applied (Figure 1 A). This nanometer-sized patch of the cell membrane can be approximated as flat, despite the actual cell membrane having a curved shape. To numerically model this scenario, we created a square prism domain with a sandwich-like structure, where the cell membrane is centrally positioned between the extracellular space and the cytoplasm. We implemented this model in COMSOL Multiphysics 6.0 using the finite element method to solve the governing equations for electrostatics, Joule heating, and conductive heat transfer.

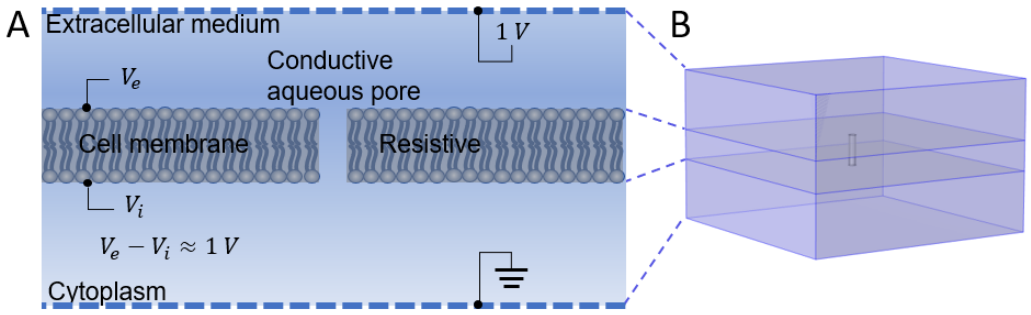

Figure 1 Schematic diagram of electroporated cell membrane with transmembrane voltage of $1\ V$ (A) and its 3D geometric implementation (B).

2.2 Boundary conditions

The initial electrical potential of the entire simulation domain was set to 0 V, and the outer surface of the domain was electrically isolated. Transmembrane voltage (TMV) thresholds ranging from a few hundred millivolts to approximately one volt have been reported to induce electroporation[25–27]. In this study, we set the top surface of the extracellular medium to 1 V for 100 µs duration and the bottom surface of the cytoplasm to 0 in the electric field, resulting in a TMV of approximately 1 V. This corresponds to the maximum TMV that a cell membrane can

attain due to the short-circuiting effect induced by electroporation, regardless of the external electric field strength, and therefore represents the condition that induces the greatest Joule heating of a pore during electroporation [25–31].

The initial temperature of the domain was set to the normal average human body temperature (i.e., 37 °C). The outer surface was maintained at a constant temperature of 37 °C. To ensure that this boundary condition did not artificially reduce the simulated temperature increment induced by Joule heating, we conducted a sensitivity analysis on the width and height of the simulation domain. Based on the results, we selected a width of 40 nm for the whole simulation domain and a thickness of 10 nm for the extracellular media (i.e. the top square prism) and intracellular media (i.e. the bottom square prism). The thicknesses of the cell membrane layer (i.e. the middle square prism) was 5 nm. We also performed a mesh sensitivity analysis using the default mesh settings of COMSOL, ranging from *Normal* to *Extremely Fine*. The results showed that mesh resolution only affected the temperature rise at the onset of the electric pulse and the temperature drop at the end of the pulse in the time-dependent study of our model, while having no significant impact on the results of the static study. The final mesh contained 1,395,808 elements with 1,886,703 degrees of freedom for Electrical Potential and Temperature respectively, under the Extremely Fine mesh setting.

2.3 Pores geometry and density

The "electropore" was modelled as a cylindrical structure with either straight or curved side across the middle of the cell membrane (Figure 1 B). We assumed the pore radius in the cell membrane is twice the average pore radius for an artificial membrane (i.e., 0.32 nm) and set it to 0.64 nm in this study [32]. To model different pore geometry, we considered both straight cylindrical pores and cylindrical pores with arc-shaped sides. For arc-shaped pores, curvature, defined as the inverse of the arc radius, was used to characterize the degree of bending of the pore wall. The top and bottom surface radii of the curved cylindrical pore remain aligned with those of the straight cylindrical pore, ranging from 0.2 nm to 1.4 nm, while the radius at the midsection of the pore is maintained at 0.2 nm, resulting in curvature values ranging from 0 to 0.316 nm^{-1}.

The cell membrane size in the simulation domain was 40 nm × 40 nm with a thickness of 5 nm, resulting in a pore density of 6.25×10^{14} $1/m^2$ when a single pore was present. The value is significantly higher than the experimentally observed pore density of 2.75×10^{10} $1/m^2$ [32]. We chose this extremely high pore density to critically assess the extreme thermal increment under such extreme condition. To model different pore densities, we increased the number of pores on the cell membrane within the simulation domain, maintaining a 5 nm spacing between pores.

2.4 Joule heating and heat transfer

In this study, Joule heating results from the electric field and serves as the only source of thermal conduction. The electrothermal coupling physics is governed by

$$\rho C_p \frac{\partial T}{\partial t} = \nabla \cdot k\nabla T + Q_e \quad (1)$$

$\rho C_p(\partial T/\partial t)$ is the item associated with cumulative temperature, where ρ is the density of the material, C_p is the specific heat capacity, T is the spatiotemporal temperature. $\nabla \cdot k\nabla T$ is the item associated with conductive temperature, where k is the thermal conductivity. Q_e is the heat source, Joule heating, with the differential form of Joule heating, giving the power per unit volume,

$$Q_e = J \cdot E \tag{2}$$

where J is the current density given by

$$J = \sigma E + J_e \tag{3}$$

where σ is the electrical conductivity, J_e is the external current density source which came from a boundary potential in our study, and E is the electric field generated by solving the governing equation,

$$\nabla \cdot (\sigma - \nabla\phi) = 0 \tag{4}$$

All parameters related to electrical and thermal properties are listed in Table 1. The specific heat capacity, mass density, and thermal conductivity of the aqueous pore, extracellular medium, and cytoplasm are assumed to be the same as water, given that the cytoplasm contains over 70% water, while the extracellular medium contains approximately 99% water. The 'electropore' is filled with a mixture of the extracellular medium and cytoplasm, so its electrical conductivity is assigned the average of the extracellular and intracellular conductivity values.

Table 1 Electrophysical and thermophysical parameters of each component.

Property	Cell membrane	Aqueous pore	Extracellular medium	Cytoplasm
Electrical conductivity, S/m	2.5×10^{-7} [33]	1 [a]	1.5 [34]	0.5 [25]
Specific heat capacity, J/(kg·K)	2000 [35,36]	4180 [b]	4180 [b]	4180 [b]
Density, kg/m^3	1100 [37]	1000 [b]	1000 [b]	1000 [b]
Thermal conductivity, W/(m·K)	0.2 [38–40]	0.6 [b]	0.6 [b]	0.6 [b]

[a] Electrical conductivity of pore is set as the mean value of the sum of extracellular and intracellular conductivity.

[b] The marked thermophysical properties are the same as water, these values have been applied in the skin electroporation simulation [37].

3. Results

3.1 The temperature increment drops within 1 μs after the cessation of the electric pulse.

We selected two points to monitor temperature changes: one at the centre of the pore (i.e., point a) and another located on the membrane, 1 nm away from the centre in the same horizontal plane (i.e., point b) (Figure 2 A). Temperature increment at point a shows an immediate increase from 0 to 0.043 °C within 1 μs as the electrical pulse was applied, and an immediate decrease to 0 within 1 μs after the pulse ended. After the initial drastic rise, the temperature remains constant. The temperature increment at point b is lower, reaching 0.03 °C. However, it exhibits the same trend, with a rapid rise at the beginning of the pulse, a sharp decline at the end, and no significant increase during the electric pulse (Figure 2 B).

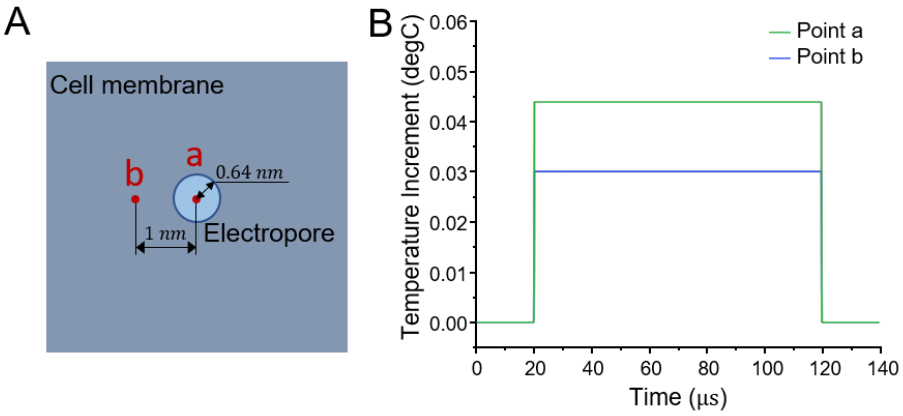

Figure 2 Dynamic temperature increment during the application of an electric pulse from 20 μs to 120 μs. (A) The schematic diagram of two chosen monitoring points. (B) The monitored temperature increments.

3.2 Spatial profiles of temperature elevation as a function of pore size.

Given the rapid onset and decay of temperature increases observed during the 100 μs pulse (Figure 2 B), we chose to model a worst-case scenario corresponding to very long pulses. All results presented hereafter are based on steady-state thermal simulations (i.e., assuming field exposures of infinite duration).

The simulated results of a straight cylindrical pore with radius of 0.64 nm show that the temperature increment decreases from the centre of the pore to the edge of the cell membrane, both horizontally and vertically. The centre point of the pore on the middle horizontal cross-section exhibits the highest temperature increment, 0.042 ^{o}C Figure 3 A and C).

With pore radii ranging from 0.2 nm to 1.4 nm, we simulated the temperature increment relative to the distance from the centre of the pore. Horizontally, the temperature increment decreases from the highest value (over 0.08 °C) at the centre of the pore to nearly 0 within 10 nm from the centre. Vertically, the temperature increment decreases from the highest value at the centre point of the pore to approximately 0 as it moves from the centre to the edge of the cell membrane. As the pore radius increases, the temperature increment rises correspondingly. The temperature increments at the centre of the pore were as follows: 0.009 °C for 0.2 nm radius, 0.024 °C for 0.4 nm radius, 0.039 °C for 0.6 nm radius, 0.052 °C for 0.8 nm radius, 0.063 °C for 1.0 nm radius, 0.072 °C for 1.2 nm radius, and 0.08 °C for 1.4 nm radius respectively, with the highest temperature increment observed for the 1.4 nm radius pore.

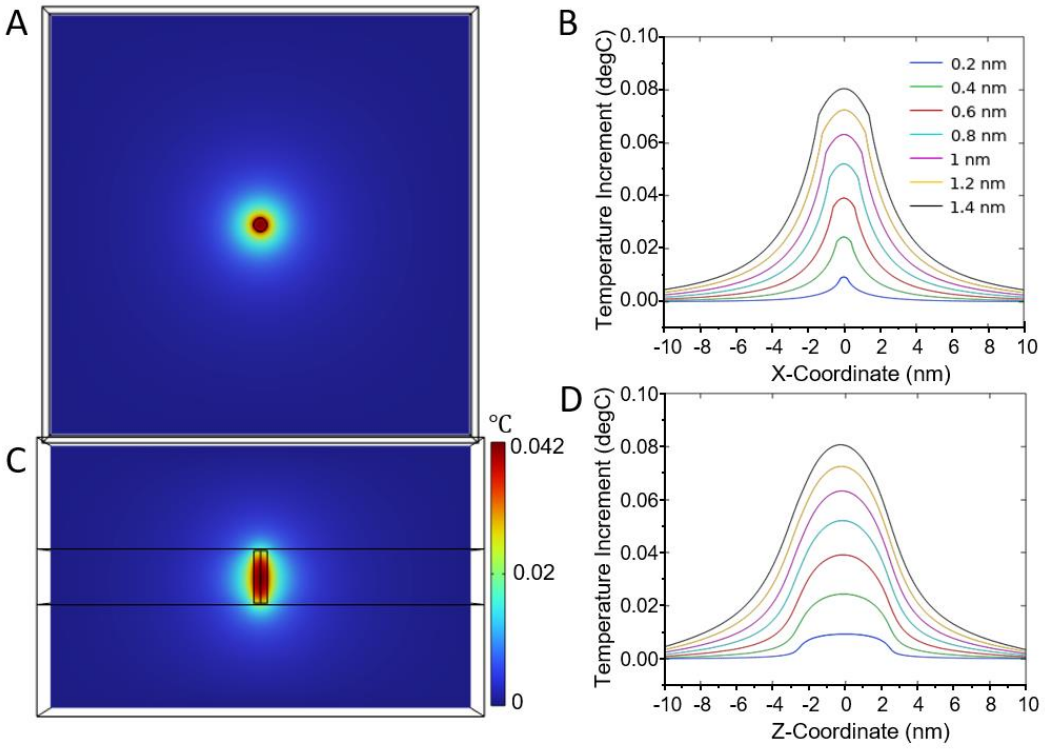

Figure 3 Temperature increments during electroporation relative to pore size. (A) The temperature increment distribution on the middle horizontal cross-section of the cell membrane. (B) The temperature increment of different pore radius from 0.2 nm to 1.4 nm along a horizontal line from 10 nm on the left to 10 nm on the right of the center point of the pore. (C) The temperature increment distribution on the middle vertical cross-section of the pore. (D) The temperature increment of different pore radius from 0.2 nm to 1.4 nm along a vertical line from 10 nm below to 10 nm above the middle point of the pore.

3.3 Curved shape of the pore increases temperature increment.

For both curved and cylindrical pores, the temperature increment increases with the top/bottom surface radius (Figure 4). At any top/bottom radius, the temperature increment is higher for cylindrical pores than for curved pores, which rises more steeply, reaching approximately 0.08 °C for cylindrical pores at a surface radius of 1.4 nm, while it is slightly below 0.06 °C for curved pores at the same radius. Specifically, the temperature increments is 0.009 °C for both cylinder pore and curved pore at 0.2 radius, 0.024 °C for cylinder pore and 0.022 °C for curved pore at radius of 0.4 nm, 0.039 °C for cylinder pore and 0.032 °C for curved pore at radius of 0.6 nm, 0.052 °C for cylinder pore and 0.041 °C for curved pore at radius of 0.8 nm, 0.063 °C for cylinder pore and 0.048 °C for curved pore at radius of 1.0 nm, 0.072 °C for cylinder pore and 0.054 °C for curved pore at radius of 1.2 nm. All the curved pores have the higher temperature increment than 0.2-nm radius cylinder pores even though they have the same pore radius of 0.2-nm on the middle horizontal cross-section of the pore, which is aligned with the results of pore size in the section 3.2.

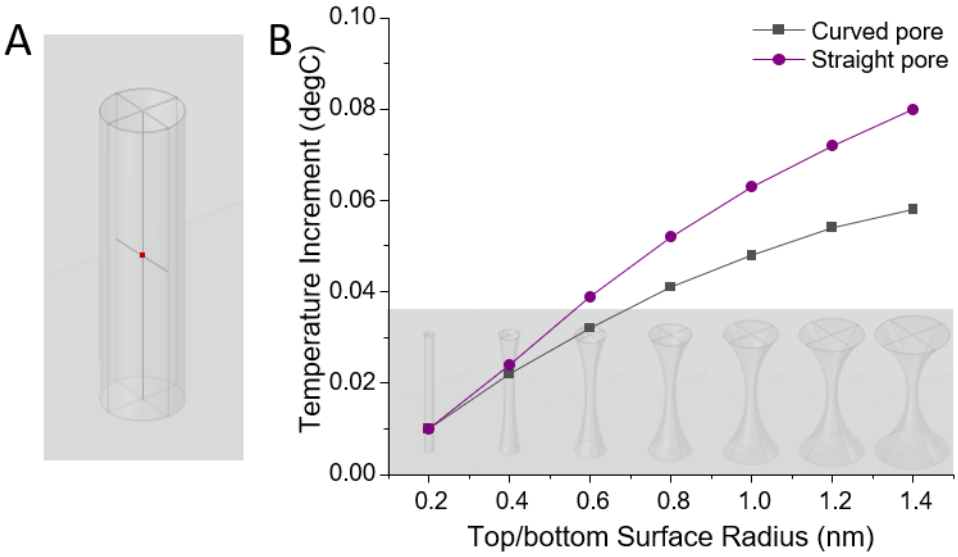

Figure 4 Temperature increment for cylinder pore and curved pore. (A) A 3D schematic representation of a cylinder pore structure with a red dot indicating where the temperature increment is measured. (B) The temperature increment of the center point in the cylinder pore and curved pore. The inset at the bottom represents the curved pore with different curvature transitioning with top/bottom surface radius. The corresponding list of surface radius to curvature is 0.2 nm: 0, 0.4 nm: 0.0625 1/nm, 0.6 nm: 0.125 1/nm, 0.8 nm: 0.182 1/nm, 1.0 nm: 0.233 1/nm, 1.2 nm: 0.275 1/nm, 1.4 nm: 0.312 1/nm.

3.4 Pore density increases the temperature increment.

The simulation results from the previous section were performed with pore density 6.25×10^{14} 1/m^2. The temperature increment at the centre point of the pore was 0.041 °C with this pore density, while the temperature increment increased to 0.045 °C with pore density 1.25×10^{15} 1/m^2, 0.048 °C with pore density 1.875×10^{15} 1/m^2, and 0.054 °C with pore density 3.125×10^{15} 1/m^2 (Figure 5). As shown by the results, although the temperature increment rose significantly with higher pore density, the maximum temperature increment remained below 0.1 °C, even under conditions where the pore-to-pore distance was extremely short compared to realistic biological setting. What deserves to be noticed from the results is that the temperature increase in the area between the pores was significant, and the total area of temperature rise exceeded that of a single pore.

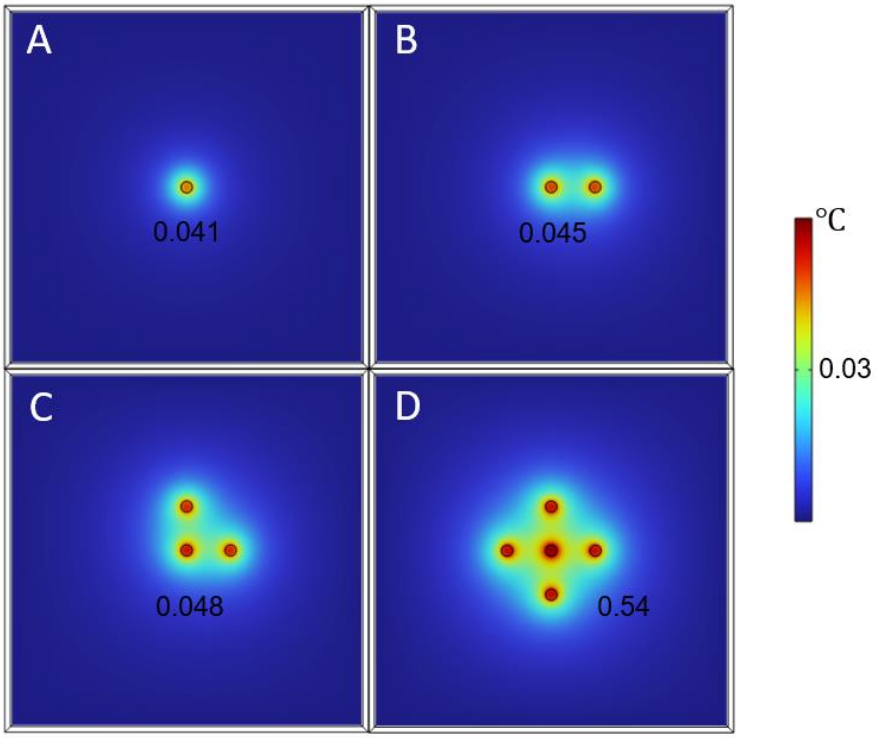

Figure 5 The temperature increment distribution on cell membrane with different pore density, (A) 1 pore: 6.25×10^{14} 1/m^2, (B) 2 pores: 1.25×10^{15} 1/m^2, (C) 3 pores: 1.875×10^{15} 1/m^2 and (D) 5 pores: 3.125×10^{15} 1/m^2. The area of the cell membrane in the simulation domain is 1600 nm^2. The vertical and horizontal distances between pores are 5 nm. Numbers below the pores indicate the largest temperature of the pore.

4. Discussion

The aim of this study was to investigate whether the Joule heating, resulting from the facilitation of electrical current through "electropores" during electroporation, could contribute to the increase in cell membrane permeability. To address this, we conducted a series of numerical simulations to model the thermal behaviour of an electroporated cell membrane patch under an applied electric field. In a time-dependent sub-study, we analysed the dynamic temperature increment over time during electric field application. In a static sub-study, we evaluated the temperature increment in relation to pore size, geometry, and density. The results indicate that (1) thermal diffusion leads to rapid temperature stabilization, occurring within fractions of a microsecond during and following the exposure, and (2) the temperature increment positively correlates with pore radius, curvature, and density. Overall, the findings of this study confirm that Joule heating induced by electroporation leads to a temperature increase; however, all observed thermal increments remain within a fraction of 0.1 °C .

A temperature increment of 0.1 °C is sufficiently small to be considered negligible in terms of its impact on maintaining the physiological functions of a cell[41–43]. For the sake of simplicity, the present study was conducted while neglecting the temperature dependence of ionic conductivity. However, it should be noted that incorporating this dependence does not alter the overall conclusions. In our preliminary simulations, the temperature dependence of electrical conductivity, σ, was modelled using the following linear approximation[44],

$$\sigma = \sigma_0 \times \left(1 + \partial \times (T - T_0)\right) \tag{5}$$

Where σ_0 is the electrical conductivity at T_0, and ∂ is the temperature coefficient. Assuming $\partial = 1.7\ (1/degC)$ for all model components, the maximum observed temperature rise was 0.090 °C for a straight cylindrical pore with 1.4 nm radius.

The specific mechanism of this Joule heating on a patch of electroporated cell membrane primarily arises from the preferential flow of current through highly conductive pores, which directs the current toward the electrically resistive lipids bilayer regions surrounding the pores. This mechanism also partially accounts for Joule heating in skin electroporation, where pore formation and localized permeability increases occur within µm-sized regions of the stratum corneum. However, the stratum corneum, which has a thickness of 10 to 50 µm and consists of 15 to 20 layers of corneocytes that have undergone complete keratinocyte differentiation and programmed cell death, exhibits different electrical and thermal conduction properties compared to the membranes of a normal cell [45,46]. Moreover, due to the markedly different geometrical scale, heat diffusion plays a fundamentally different role in the thermal dynamics. This fundamental difference explains the much smaller temperature increase observed at the pore level in this study, which remains within a fraction of 0.1 °C, in contrast to the substantial temperature increment of up to 30 °C observed in skin electroporation under prolonged electric pulses. Once the temperature of lipids bilayer reaches 65 °C, a phase transition is induced, enhancing permeability of the stratum corneum surrounding the pores [47]. Therefore, unlike skin electroporation, normal cell membrane electroporation does not attribute the increase in permeability during electroporation to Joule heating resulting from the facilitation of electric current through “electropores”.

This conclusion is limited to the scale of an electroporated patch of the cell membrane. At this scale, the small thermal mass facilitates rapid heat dissipation into the surrounding lipid bilayer and aqueous environment. In this study, the boundary temperature of the membrane patch was maintained at a constant 37 °C, and the high thermal conductivity of water promoted efficient heat diffusion, preventing long-term heat accumulation. Our results is also compatible with the joule heat occurring in channel proteins [48].

5. Conclusion

The results of this study indicate that Joule heating, resulting from the increased current density through pores formed during electroporation, leads to local temperature increases in the cell membrane. However, the observed temperature rise is on the order of a fraction of 0.1°C. Even though this temperature increase does escalate with pore size, curvature, and density, it remains insufficient to cause significant alterations to the lipid structure or to induce phase transitions capable of affecting membrane permeability. This study therefore suggests that Joule heating in the vicinity of electropores does not play a primary role in the increase of cell membrane permeability during electroporation.

Acknowledgments

The authors are grateful to the anonymous reviewers for their constructive feedback.

Authorship confirmation statement

Ting Shu: Conceptualization, Methodology, Writing – Original Draft.

Quim Castellví: Conceptualization, Methodology.

Antoni Ivorra: Conceptualization, Writing - Review & Editing, Funding acquisition, Supervision

Authors' disclosure statements

The authors declare no known competing financial interests or personal relationships that could have appeared to influence the work reported in this paper.

Funding statement

This work was financially supported by the Agencia Estatal de Investigación, Plan Estatal de Investigación Científica,Técnica y de Innovación under Grant PID2023-149699OB-I00.

Reference

1. Melikov KC, Frolov VA, Shcherbakov A, et al. Voltage-Induced Nonconductive Pre-Pores and Metastable Single Pores in Unmodified Planar Lipid Bilayer. Biophysical Journal 2001;80(4):1829–1836; doi: 10.1016/S0006-3495(01)76153-X.

2. Sengel JT, Wallace MI. Imaging the dynamics of individual electropores. Proceedings of the National Academy of Sciences 2016;113(19):5281–5286; doi: 10.1073/pnas.1517437113.

3. Weaver JC, Chizmadzhev YuA. Theory of electroporation: A review. Bioelectrochemistry and Bioenergetics 1996;41(2):135–160; doi: 10.1016/S0302-4598(96)05062-3.

4. DeBruin KA, Krassowska W. Modeling Electroporation in a Single Cell. I. Effects of Field Strength and Rest Potential. Biophysical Journal 1999;77(3):1213–1224; doi: 10.1016/S0006-3495(99)76973-0.

5. Levine ZA, Vernier PT. Life Cycle of an Electropore: Field-Dependent and Field-Independent Steps in Pore Creation and Annihilation. J Membrane Biol 2010;236(1):27–36; doi: 10.1007/s00232-010-9277-y.

6. Sözer EB, Haldar S, Blank PS, et al. Dye Transport through Bilayers Agrees with Lipid Electropore Molecular Dynamics. Biophysical Journal 2020;119(9):1724–1734; doi: 10.1016/j.bpj.2020.09.028.

7. Shirakashi R, Sukhorukov VL, Tanasawa I, et al. Measurement of the permeability and resealing time constant of the electroporated mammalian cell membranes. International Journal of Heat and Mass Transfer 2004;47(21):4517–4524; doi: 10.1016/j.ijheatmasstransfer.2004.04.007.

8. Pucihar G, Kotnik T, Teissié J, et al. Electropermeabilization of dense cell suspensions. Eur Biophys J 2007;36(3):173–185; doi: 10.1007/s00249-006-0115-1.

9. Mercadal B, Vicente R, Ivorra A. Pulsed radiofrequency for chronic pain: In vitro evidence of an electroporation mediated calcium uptake. Bioelectrochemistry 2020;136:107624; doi: 10.1016/j.bioelechem.2020.107624.

10. Sözer EB, Pocetti CF, Vernier PT. Asymmetric Patterns of Small Molecule Transport After Nanosecond and Microsecond Electropermeabilization. J Membrane Biol 2018;251(2):197–210; doi: 10.1007/s00232-017-9962-1.

11. Ivorra A, Rubinsky B. In vivo electrical impedance measurements during and after electroporation of rat liver. Bioelectrochemistry 2007;70(2):287–295; doi: 10.1016/j.bioelechem.2006.10.005.

12. Cukjati D, Batiuskaite D, André F, et al. Real time electroporation control for accurate and safe in vivo non-viral gene therapy. Bioelectrochemistry 2007;70(2):501–507; doi: 10.1016/j.bioelechem.2006.11.001.

13. López-Alonso B, Sarnago H, Burdío JM, et al. Multiple Output Inverter and Monitoring System for Homogeneous Electroporation. IEEE Transactions on Power Electronics 2023;38(2):1935–1947; doi: 10.1109/TPEL.2022.3212783.

14. Serša I, Kranjc M, Miklavčič D. Current density imaging sequence for monitoring current distribution during delivery of electric pulses in irreversible electroporation. BioMed Eng OnLine 2015;14(S3):S6; doi: 10.1186/1475-925X-14-S3-S6.

15. Neumann E, Toensing K, Kakorin S, et al. Mechanism of electroporative dye uptake by mouse B cells. Biophys J 1998;74(1):98–108; doi: 10.1016/S0006-3495(98)77771-9.

16. Pakhomov AG, Bowman AM, Ibey BL, et al. Lipid nanopores can form a stable, ion channel-like conduction pathway in cell membrane. Biochemical and Biophysical Research Communications 2009;385(2):181–186; doi: 10.1016/j.bbrc.2009.05.035.

17. Rems L, Viano M, Kasimova MA, et al. The contribution of lipid peroxidation to membrane permeability in electropermeabilization: A molecular dynamics study. Bioelectrochemistry 2019;125:46–57; doi: 10.1016/j.bioelechem.2018.07.018.

18. Denet A-R, Vanbever R, Préat V. Skin electroporation for transdermal and topical delivery. Advanced Drug Delivery Reviews 2004;56(5):659–674; doi: 10.1016/j.addr.2003.10.027.

19. Pliquett UF, Vanbever R, Preat V, et al. Local transport regions (LTRs) in human stratum corneum due to long and short `high voltage' pulses. Bioelectrochemistry and Bioenergetics 1998;47(1):151–161; doi: 10.1016/S0302-4598(98)00180-9.

20. Pliquett UF, Gusbeth CA. Perturbation of human skin due to application of high voltage. Bioelectrochemistry 2000;51(1):41–51; doi: 10.1016/S0302-4598(99)00070-7.

21. Tekle E, Astumian RD, Friauf WA, et al. Asymmetric Pore Distribution and Loss of Membrane Lipid in Electroporated DOPC Vesicles. Biophysical Journal 2001;81(2):960–968; doi: 10.1016/S0006-3495(01)75754-2.

22. Saulis G. Cell electroporation: Part 3. Theoretical investigation of the appearance of asymmetric distribution of pores on the cell and their further evolution. Bioelectrochemistry and Bioenergetics 1993;32(3):249–265; doi: 10.1016/0302-4598(93)80049-Z.

23. Batista Napotnik T, Miklavčič D. Pulse Duration Dependent Asymmetry in Molecular Transmembrane Transport Due to Electroporation in H9c2 Rat Cardiac Myoblast Cells In Vitro. Molecules 2021;26(21):6571; doi: 10.3390/molecules26216571.

24. Tarek M. Membrane electroporation: a molecular dynamics simulation. Biophys J 2005;88(6):4045–4053; doi: 10.1529/biophysj.104.050617.

25. Hibino M, Itoh H, Kinosita K. Time courses of cell electroporation as revealed by submicrosecond imaging of transmembrane potential. Biophysical Journal 1993;64(6):1789–1800; doi: 10.1016/S0006-3495(93)81550-9.

26. Pucihar G, Miklavcic D, Kotnik T. A time-dependent numerical model of transmembrane voltage inducement and electroporation of irregularly shaped cells. IEEE Trans Biomed Eng 2009;56(5):1491–1501; doi: 10.1109/TBME.2009.2014244.

27. Ivorra A, Villemejane J, Mir LM. Electrical modeling of the influence of medium conductivity on electroporation. Phys Chem Chem Phys 2010;12(34):10055; doi: 10.1039/c004419a.

28. Kinosita K, Ashikawa I, Saita N, et al. Electroporation of cell membrane visualized under a pulsed-laser fluorescence microscope. Biophysical Journal 1988;53(6):1015–1019; doi: 10.1016/S0006-3495(88)83181-3.

29. Weaver JC. Electroporation in cells and tissues: A biophysical phenomenon due to electromagnetic fields. Radio Science 1995;30(1):205–221; doi: 10.1029/94RS01160.

30. Weaver JC. Electroporation of cells and tissues. IEEE Transactions on Plasma Science 2000;28(1):24–33; doi: 10.1109/27.842820.

31. Weaver JC. Electroporation of biological membranes from multicellular to nano scales. IEEE Transactions on Dielectrics and Electrical Insulation 2003;10(5):754–768; doi: 10.1109/TDEI.2003.1237325.

32. Lafarge EJ, Muller P, Schroder AP, et al. Activation energy for pore opening in lipid membranes under an electric field. Proceedings of the National Academy of Sciences 2023;120(11):e2213112120; doi: 10.1073/pnas.2213112120.

33. Gimsa J, Müller T, Schnelle T, et al. Dielectric spectroscopy of single human erythrocytes at physiological ionic strength: dispersion of the cytoplasm. Biophysical Journal 1996;71(1):495–506; doi: 10.1016/S0006-3495(96)79251-2.

34. Kinosita K, Tsong TY. Voltage-induced conductance in human erythrocyte membranes. Biochimica et Biophysica Acta (BBA) - Biomembranes 1979;554(2):479–497; doi: 10.1016/0005-2736(79)90386-9.

35. Heimburg T. Mechanical aspects of membrane thermodynamics. Estimation of the mechanical properties of lipid membranes close to the chain melting transition from calorimetry. Biochimica et Biophysica Acta (BBA) - Biomembranes 1998;1415(1):147–162; doi: 10.1016/S0005-2736(98)00189-8.

36. Nagle JF, Wilkinson DA. Lecithin bilayers. Density measurement and molecular interactions. Biophysical Journal 1978;23(2):159–175; doi: 10.1016/S0006-3495(78)85441-1.

37. Zorec B, Becker S, Reberšek M, et al. Skin electroporation for transdermal drug delivery: The influence of the order of different square wave electric pulses. International Journal of Pharmaceutics 2013;457(1):214–223; doi: 10.1016/j.ijpharm.2013.09.020.

38. Nakano T, Kikugawa G, Ohara T. A molecular dynamics study on heat conduction characteristics in DPPC lipid bilayer. J Chem Phys 2010;133(15):154705; doi: 10.1063/1.3481650.

39. Kvadsheim PH, Folkow LP, Blix AS. Thermal conductivity of minke whale blubber. Journal of Thermal Biology 1996;21(2):123–128; doi: 10.1016/0306-4565(95)00034-8.

40. Youssefian S, Rahbar N, Van Dessel S. Thermal conductivity and rectification in asymmetric archaeal lipid membranes. The Journal of Chemical Physics 2018;148(17):174901; doi: 10.1063/1.5018589.

41. Heimburg T. Physical Properties of Biological Membranes. In: Digital Encyclopedia of Applied Physics. (Wiley-VCH Verlag GmbH & Co. KGaA. ed) Wiley; 2009; doi: 10.1002/3527600434.eap674.

42. Quinn PJ. Effects of temperature on cell membranes. Symp Soc Exp Biol 1988;42:237–258.

43. Balogh G, Péter M, Glatz A, et al. Key role of lipids in heat stress management. FEBS Letters 2013;587(13):1970–1980; doi: 10.1016/j.febslet.2013.05.016.

44. Neal II RE, Garcia PA, Robertson JL, et al. Experimental Characterization and Numerical Modeling of Tissue Electrical Conductivity during Pulsed Electric Fields for Irreversible Electroporation Treatment Planning. IEEE Transactions on Biomedical Engineering 2012;59(4):1076–1085; doi: 10.1109/TBME.2012.2182994.

45. Wu KS, van Osdol WW, Dauskardt RH. Mechanical properties of human stratum corneum: Effects of temperature, hydration, and chemical treatment. Biomaterials 2006;27(5):785–795; doi: 10.1016/j.biomaterials.2005.06.019.

46. Becker S. Transport modeling of skin electroporation and the thermal behavior of the stratum corneum. International Journal of Thermal Sciences 2012;54:48–61; doi: 10.1016/j.ijthermalsci.2011.10.022.

47. Becker S. Modeling Transdermal Delivery by Electroporation: The Thermodynamic Approach. In: Handbook of Electroporation. (Miklavčič D. ed) Springer International Publishing: Cham; 2017; pp. 1219–1235; doi: 10.1007/978-3-319-32886-7_14.

48. Wazawa T, Nagai T. Joule heating involving ion currents through channel proteins. Biophys Physicobiol 2023;20(3):e200030; doi: 10.2142/biophysico.bppb-v20.0030.